Electronic Supplementary Material (ESI) for Energy & Environmental Science
This journal is © The Royal Society of Chemistry 2012

Supplementary Information for The Carbon Abatement Potential of High Penetration Intermittent Renewables

Elaine K. Hart*[a] and Mark Z. Jacobson[a]

1 Model updates

A number of improvements were made to the scheduling and dispatch model used in this study since the publication of [Hart and Jacobson(2011)]. These changes are described below.

1.1 Wind Power Statistical Model

The statistical model for wind power employed in [Hart and Jacobson(2011)] relied on the application of a power curve to simulated wind speeds at each site in order to approximate the output of wind power from each farm. This model used a single average wind speed at each time step for each site in order to reduce computational complexity. This approximation was later found to overestimate the wind power produced in aggregate, when compared to the predicted wind power output supplied in the Western Wind Dataset [3TIER(2010)]. To improve the treatment of wind power, an autoregressive-like model was developed for the forecast error of the total aggregated wind power output (the sum of the power output reported for each site in the dataset). In the updated model, the normalized aggregated wind power, $g(t)$ is approximated from the forecasted wind power, $\hat{g}(t)$ according to:

$$g(t) = \hat{g}(t) + \beta \left[g(t-1) - \hat{g}(t) \right] + \tilde{y} \tag{1}$$

where β is the autocorrelation coefficient of the input wind power signal and $\tilde{y}$ is a random variable with a symmetrically truncated distribution based on a normal distribution with mean 0 and variance σ_g^2. The distribution is truncated in order to ensure that $g(t)$ is on the interval $[0, 1]$. This approach breaks down when one of

[a] *Department of Civil and Environmental Engineering, Stanford University, Stanford, CA, 94305. Fax: +1 650 723 7058; Tel: +1 650 721 2650; E-mail: ehart@stanford.edu*

the following inequalities holds:

$$\hat{g}(t) + \beta\left[g(t-1) - \hat{g}(t-1)\right] < 0 \tag{2}$$

$$\hat{g}(t) + \beta\left[g(t-1) - \hat{g}(t-1)\right] > 1 \tag{3}$$

If the first inequality holds, $g(t)$ is set to 0 and if the second inequality holds, $g(t)$ is set to 1. In the k^{th} realization, the available wind power, P_w^{max}, is calculated from the k^{th} normalized wind power signal, $g(k,t)$ and the installed capacity, W according to:

$$P_w^{max}(t) = W \times g(k,t) \tag{4}$$

Capping introduces a small bias in the final wind power signal. This bias is removed by scaling all values of $P_w^{max}(k,t)$ by a constant so that the mean wind power availability across all realizations and all times is equal to the mean forecasted wind power output. The input wind power signal (from the Western Wind Dataset[3TIER(2010)]) is taken as the day-ahead forecasted wind power output.

The forecast error distribution produced by this method depends on the parameter, σ_g. In this analysis, both the wind and solar power forecasts are assumed to have a 10% day-ahead RMS error. This is achieved for wind power by comparing the RMS wind power error associated with 10GW of installed wind power for various values of σ_g. This analysis (shown in Figure 1) yielded a value of $\sigma_g \approx 0.16$.

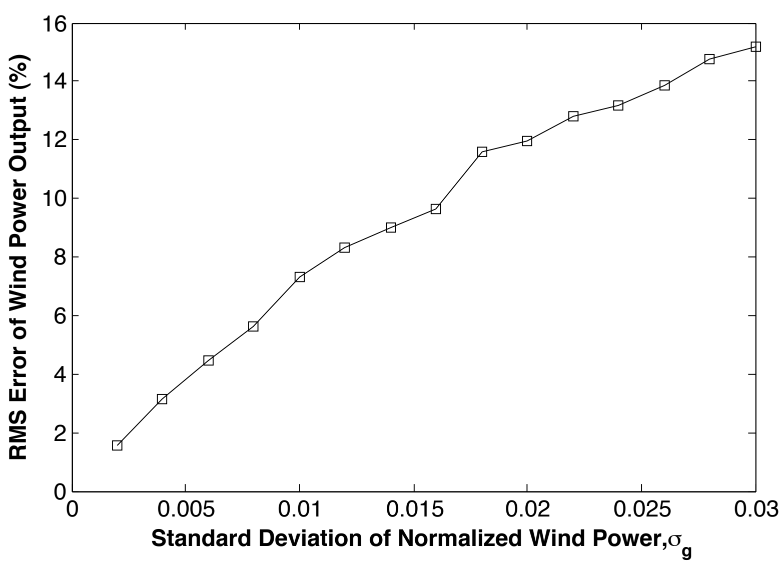

Figure 1 Wind power forecast error trials for determining σ_g. The value of σ_g is chosen so that the RMS error of the day-ahead forecast is approximately 10%.

1.2 Irradiance Statistical Model

The updated irradiance model assumes that the forecast error in the direct normal irradiance, I^{DNI} can be modeled by an autoregressive-like process:

$$I_i^{DNI}(t) = \hat{I}_i^{DNI}(t) + \kappa \left[I_i^{DNI}(t-1) - \hat{I}_i^{DNI}(t-1) \right] + \tilde{b}_i \tag{5}$$

where $\hat{I}_i^{DNI}$ is the forecasted direct normal irradiance at site i, ϕ is the autocorrelation coefficient, and $\tilde{b}_i \sim \mathcal{N}(0, \sigma_{DNI}^2)$ are correlated random variables, based on the site-site correlations present in the input dataset. Irradiance data from the National Solar Radiation Database (NSRDB) [Wilcox and Marion(2007)] was used in this analysis. At each time step, $I_i^{DNI}(t)$ is capped so that it is necessarily non-negative. After producing all realizations, $I_i^{DNI}(t)$ is again capped so that it never exceeds the maximum observed DNI in each hour of the year, based on data from 1991 to 2005.

The diffuse horizontal irradiance (DHI) is calculated directly from the DNI, assuming an affine relationship between the two variables that depends on the hour of the year. Several plots of the DHI versus the DNI for given hours of the year (over multiple years and multiple sites) indicated that the relationship is substantially different in low- and high-DNI regimes and that the DHI peaks at some DNI, separating the two regime (see Figure 2). The data is therefore separated into two regimes in order to approximate the DHI:

$$I_i^{DHI}(t) = \begin{cases} c_1(t) I_i^{DNI}(t) + b_1(t) & I_i^{DNI}(t) \leq I^*(t) \\ c_2(t) I_i^{DNI}(t) + b_2(t) & I_i^{DNI}(t) > I^*(t) \end{cases} \tag{6}$$

where t is the hour of the year; the fit parameters $c_1(t)$, $c_2(t)$, $b_1(t)$, and $b_2(t)$ are selected using a least-squares fit to the data at all stations over the years 1991-2005; and $I^*(t)$ is the value of the DNI corresponding to the maximum DHI in hour t across all years, which serves as an approximation for the boundary between the two DHI regimes. The DHI is also capped between 0 and the maximum observed DHI in each hour of the year over several years of NSRDB data to ensure reasonable values. An example of the resulting fit function for the DHI is illustrated for 12:00pm on April 10th in Figure 2. Note that the data shown reflect only 2000-2005, but the fits used in the simulations include years 1991-1999 as well.

With the DNI and the DHI, the global horizontal irradiance (GHI) can be approximated according to:

$$I_i^{GHI}(t) = I_i^{DNI}(t) sin\beta_i(t) + I_i^{DHI}(t) \tag{7}$$

where β is the solar altitude angle, a function of both location and time. Since errors in the GHI are often reported, the GHI is used to choose the value of σ_{DNI}

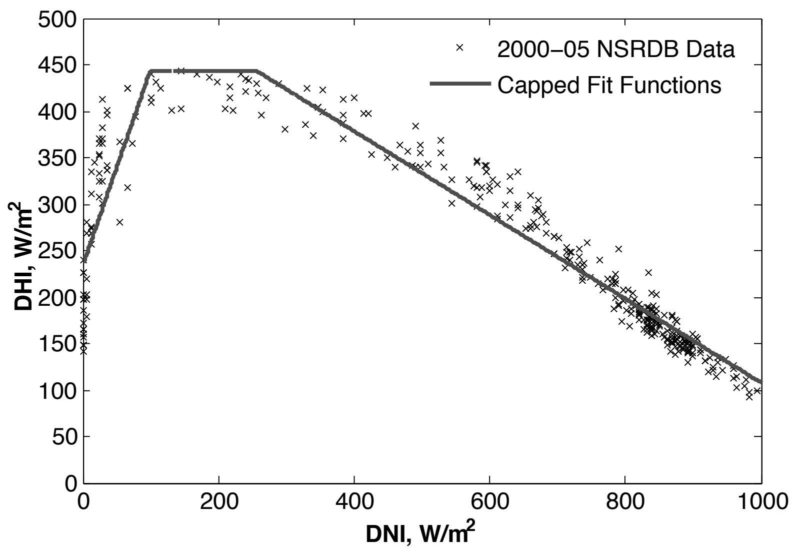

Figure 2 Irradiance data at 12:00pm on April 10th at all California sites from the NSRDB over 2000-2005, plotted with the corresponding two-regime fit described in Eq. 6, with capping of values that exceed the maximum DHI in the dataset.

that provides the appropriate day-ahead forecast uncertainty. An analysis of the effect of varying σ_{DNI} on the RMS error of the GHI is shown in Figure 3. A value of $\sigma_{DNI} = 130\text{W/m}^2$ was chosen so that the RMS error of the GHI over the simulation period was approximately 10%.

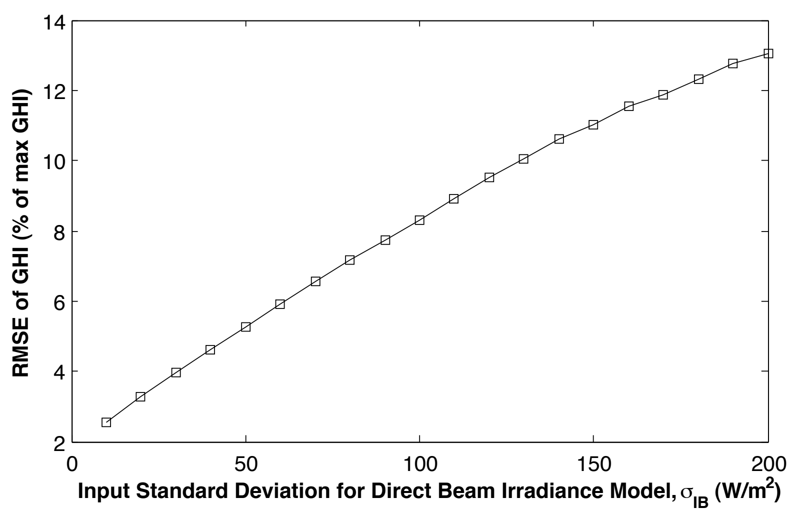

Figure 3 Solar thermal power forecast error trials for determining σ_{IB}. The value of σ_{DNI} is chosen so that the RMS error of the day-ahead forecast is approximately 10%.

Electronic Supplementary Material (ESI) for Energy & Environmental Science
This journal is © The Royal Society of Chemistry 2012

1.3 Irradiance Data

The simulations in [Hart and Jacobson(2011)] used irradiance data from the SolarAnywhere database [Clean Power Research, LLC(2010)] for the year 2006. However, slight differences in the sunrise and sunset times were found between the models employed for the NSRDB and the SolarAnywhere data. Because the NSRDB historical dataset was used to approximate upper bounds for the DNI and the DHI, this discrepancy led to unrealistic capping of the DNI and the DHI in some hours near the sunrise or sunset over 2006. In order to avoid this issue, irradiance data was modeled for 2006 in this analysis by scaling each day of the 2005 DNI time series data by the ratio of the 2006 mean daily GHI to the 2005 mean daily GHI and capping with the historical maximum DNI to ensure reasonable values. This method maintains the general meteorological conditions from the 2006 dataset, but mimics the cloud-cover temporal patterns from the 2005 dataset.

1.4 CSP Constraints

The CSP model was also updated in order to better account for the flexibility of the curtailment controls. In real parabolic trough systems, curtailment can be achieved by rotating the mirrors away from the sun, a process that requires movement of several large mechanical parts. It is unlikely that this cumbersome approach would be used for real-time load balancing[Mancini(2011)], so the model now assumes that reductions in the power sent to the thermal energy storage (TES) system from the solar field are scheduled on a day-ahead basis. The following constraints are included in the scheduling problem to determine the solar thermal curtailment schedule:

$$\begin{aligned}
S^{\circ}_{csp}(t) - \eta_s S^{\circ}_{csp}(t-1) = P^{\circ}_{col}(t) - \frac{P^{\circ}_{csp}(t)}{\eta_{turb}}, \qquad & \forall t \\
0 \le P^{\circ}_{col}(t) \le \eta_{col} \sum_j A_{ap}(j) I'_{col}(j,t), \quad & \forall t \\
0 \le P^{\circ}_{csp}(t) \le P^{max}_{csp}, \qquad & \forall t \\
0 \le S^{\circ}_{csp}(t) \le S^{max}_{csp}, \qquad & \forall t
\end{aligned} \tag{8}$$

where S°_{csp} is the scheduled energy stored in the TES system, P°_{col} is the scheduled power collected from all solar fields (which can be reduced from the maximum available solar power by rotating the mirrors away from the sun), P°_{csp} is the scheduled power output from all CSP systems, $A_{ap}(j)$ is the aperture area at site j, I'_{col} is the forecasted irradiance that can be collected by the parabolic troughs, P^{max}_{csp} is the maximum aggregated CSP power block capacity, S^{max}_{csp} is the maximum energy capacity of the TES system, η_S is the efficiency of the storage system, η_{col} is the collector efficiency, and η_{turb} is the turbine efficiency.

In real-time, the power sent to the TES system from the collectors, P_{col}, is uniquely determined by the scheduled mirror angle and the realized irradiance, I_{col}. P_{col} can be approximated prior to solving the dispatch problem by assuming that the scheduled mirror angle fixes the ratio of the collected energy to the irradiance:

$$\begin{aligned} P_{col}(k,t) &= \frac{P^{\circ}_{col}(t)}{\eta_{col}\sum_j A_{ap}(j) I'_{col}(j,t)} \left[\eta_{col} \sum_j A_{ap}(j) I_{col}(k,j,t) \right] \\ &= P^{\circ}_{col}(t) \frac{\sum_j A_{ap}(j) I_{col}(k,j,t)}{\sum_j A_{ap}(j) I'_{col}(j,t)} \end{aligned} \tag{9}$$

The CSP model then contributes the following constraints to the dispatch problem:

$$\begin{aligned} S_{csp}(k,t) - \eta_s S_{csp}(k,t-1) = P_{col}(k,t) - \frac{P_{csp}(k,t)}{\eta_{turb}}, &\quad \forall k,t \\ 0 \leq P_{csp}(k,t) \leq P^{max}_{csp}, &\quad \forall k,t \\ 0 \leq S_{csp}(k,t) \leq S^{max}_{csp}, &\quad \forall k,t \end{aligned} \tag{10}$$

where k is the realization and the circle superscript is dropped to indicate that the variables represent realizations or real-time dispatch, rather than schedules.

1.5 Reserve Capacity Requirements

In [Hart and Jacobson(2011)], the majority of the carbon emissions associated with high penetrations of renewables were associated with the spinning reserves required to meet the loss of load expectations constraint of 1 day in 10 years. The initial simulations assumed that a constant capacity of spinning reserves was required in every hour of the simulation (unless the reserves exceeded the forecasted load). While the resulting spinning reserve capacities far exceed the present day conventions for spinning reserves, this assumption was made in order to ensure a conservative approximation of the carbon emissions reductions associated with intermittent renewables. Furthermore, it is likely that in systems with high penetrations of intermittent renewables, the present day conventions will not ensure system reliability as they do today. New conventions, which will undoubtedly depend on the penetration of intermittent generation, must be developed for high penetration systems. Toward this end, we have included a new treatment of spinning reserves in the simulations presented in this study.

The model assumes that the system operator schedules spinning reserves to be available based on the solution of the day-ahead scheduling problem. Available

Electronic Supplementary Material (ESI) for Energy & Environmental Science
This journal is © The Royal Society of Chemistry 2012

spinning reserves in each hour, P°_{spin}, are assumed to be a linear function of the forecasted load, L', and the scheduled generation from intermittent renewables:

$$P^{\circ}_{spin}(t) = x_L L'(t) + x_R \left[P^{\circ}_{w}(t) + P^{\circ}_{csp} + P'_{pv}(t)\right] \tag{11}$$

where P°_{w} is the scheduled wind power, P°_{csp} is the scheduled CSP power, and P'_{pv} is the forecasted PV output, and x_L and x_R are constants. Spinning reserve signals are produced for various values of x_L and x_R and these signals are compared against the power deficit signal ($P_{\delta}(k,t)$, an expensive power source included in the dispatch model to ensure feasibility) in order to count the frequency of loss of load events. If the spinning reserve signal is sufficient to meet the power deficit signal in all but 0.0274% of the hours (an LOLE of 1 day in 10 years) across all realizations, then the corresponding x_L and x_R pair represent an acceptable spinning reserve scheduling strategy. The set of all acceptable spinning reserve strategies, X is therefore described by Equation 12.

$$X = \left\{(x_L, x_R) : \left|\left\{(k,t) : P^{\circ}_{spin}(t) \leq P_{\delta}(k,t)\right\}\right| \leq LOLE \times K \times T\right\} \tag{12}$$

Of all acceptable sets of x_L and x_R, the strategy is then chosen that minimizes the time-integrated spinning reserve capacity.

$$\begin{aligned} \text{minimize} \quad & \sum_{t=1}^{T} P^{\circ}_{spin}(t) \\ \text{subject to} \quad & (x_L, x_R) \in X \end{aligned} \tag{13}$$

2 Selection of the flexible generation parameter

The deterministic scheduling problem includes a constraint on the maximum amount of scheduled generation, $(1-\alpha)$, in each hour that is allowed to come from inflexible generators. Here, an inflexible generator refers to any technology that cannot be ramped down or curtailed in real-time. The model assumes that geothermal, CSP, PV, and hydroelectric generators are inflexible in this capacity so that all downward flexibility must be provided by flexible natural gas plants and curtailable wind power. These assumptions ensure that the solutions do not underestimate the natural gas capacity required to reliably meet demand or the emissions associated with the generation of natural gas plants. However the flexibility assumptions also neglect some potential contributions to system flexibility from hydroelectric plants.

The minimum fraction of scheduled generation that must be downwardly flexible (ie. from wind or natural gas), α is an operating decision that affects both the scheduling and the dispatch of the inflexible generators. For systems with CSP, where curtailment of the collected power can be scheduled on a day-ahead basis, a large α will result in CSP curtailment at lower system-wide CSP capacities, while a small α may lead to infeasibility in the dispatch problem in hours of unexpectedly high irradiance. For technologies with uncontrollable output (distributed photovoltaics and baseload generators), a large α may result in infeasibility of the scheduling problem at lower system-wide installed capacities of the technology, while a small α may lead to infeasibility in the dispatch problem in hours of high irradiance and/or low demand.

For the single-technology analyses, the sensitivities of the primary model outputs (energy penetration of the technology of interest, system-wide emissions, and total natural gas capacity) to α were investigated for low, moderate, and high capacities. These analyses were used to determine values of α for each technology that minimized the system-wide carbon dioxide emissions while ensuring the feasibility of both the scheduling and dispatch problems. Results from the wind power analysis (see Figure 4) indicate that the model outputs are not sensitive to α in modeling wind power integration because wind power can be curtailed on a real-time basis. This dramatically reduces the burden on the rest of the system to provide downward generating flexibility. Based on this analysis, a value of $\alpha = 0.3$ was chosen for all subsequent wind power simulations.

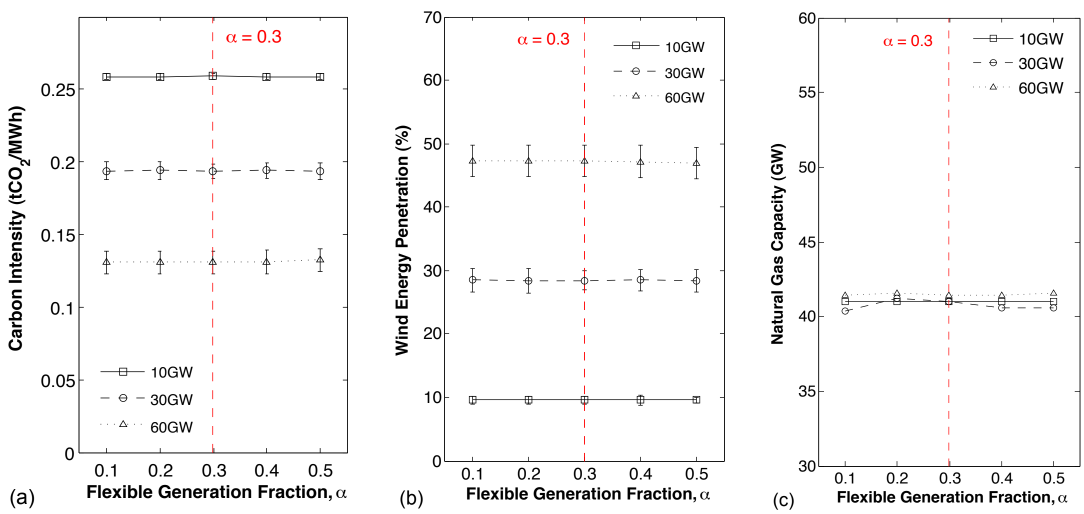

Figure 4 The sensitivity of (a) system-wide carbon intensity, (b) wind energy penetration, and (c) natural gas capacity to flexible generation fraction, α for wind scenarios, with $K = 20$. Based on these simulations, a value of $\alpha = 0.3$ (shown as red dashed line) was chosen for all subsequent wind power simulations.

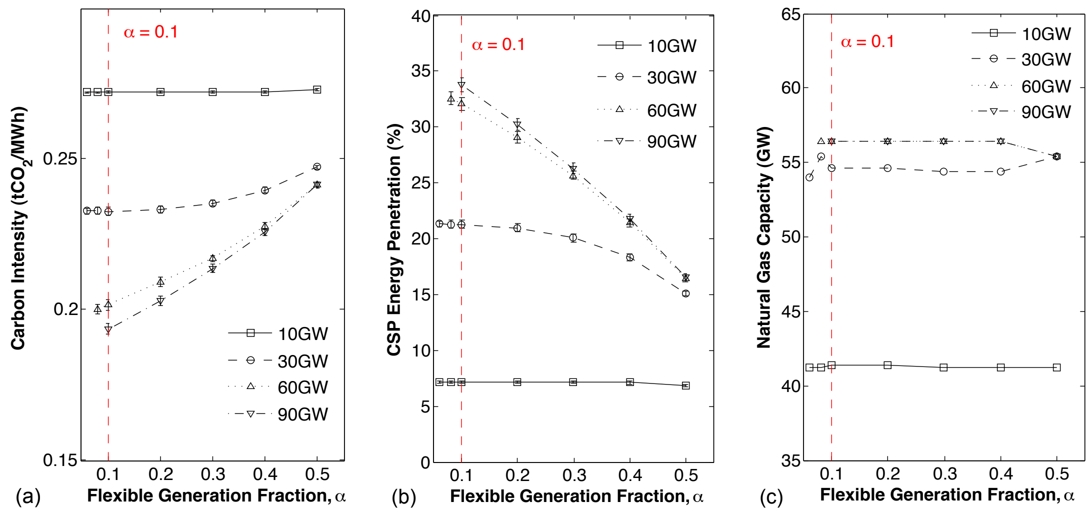

Figure 5 The sensitivity of (a) system-wide carbon intensity, (b) CSP energy penetration, and (c) natural gas capacity to flexible generation fraction, α for wind scenarios, with $K = 20$. Based on these simulations, a value of $\alpha = 0.1$ (shown as red dashed line) was chosen for all subsequent CSP simulations.

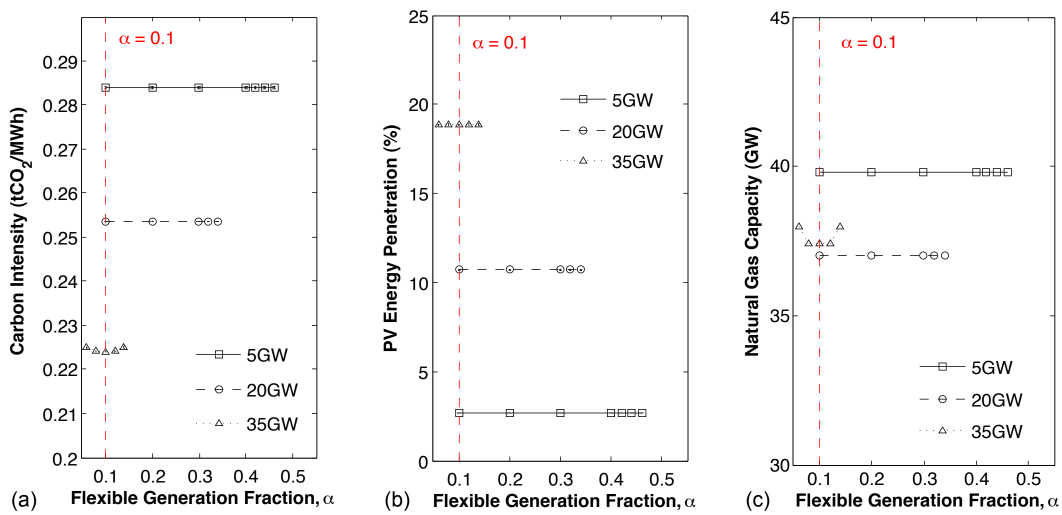

Figure 6 The sensitivity of (a) system-wide carbon intensity, (b) PV energy penetration, and (c) natural gas capacity to flexible generation fraction, α for wind scenarios, with $K = 20$. Based on these simulations, a value of $\alpha = 0.1$ (shown as red dashed line) was chosen for all subsequent PV power simulations.

Results from the CSP analysis are shown in Figure 5. For values of α smaller than those plotted, the dispatch problem is infeasible for some time steps, and for values of α greater than those plotted, the scheduling problem is infeasible. Not

Electronic Supplementary Material (ESI) for Energy & Environmental Science
This journal is © The Royal Society of Chemistry 2012

surprisingly, the sensitivity of each output to α depends on the CSP penetration, as greater penetrations require greater system-wide flexibility. At higher penetrations, the problem is both more constrained and more sensitive to α. Based on these results, a value of $\alpha = 0.1$ was chosen for all subsequent CSP simulations. At high penetrations, this is close to the feasibility limit of the dispatch problem, which ensures fairly low-emissions operation. At lower penetrations, the outputs are less sensitive to α and a value of $\alpha = 0.1$ still maintains low-emissions operation.

Results from the PV analysis are shown in Figure 6. The model outputs were largely insensitive to the value of α, particularly at small-to-moderate sized capacities. At 35GW, a value of $\alpha = 0.1$ yielded both the minimum carbon emissions and minimum natural gas capacity, so this value was chosen for all subsequent PV calculations in the single-technology analysis. In the analyses of portfolios containing both wind and solar power, PVs are modeled as curtailable in order to examine very high penetrations. For these simulations, PVs were not included in the inflexible generation fleet and α was set to 0.3, as in the wind-only simulations.

3 Natural gas utilization in wind-dominated portfolios

The natural gas utilization analysis was repeated for a portfolio with 70GW wind, 30GW solar, 9GW geothermal, and existing hydropower in order to test the sensitivity of the conclusions to the make-up of the renewable portfolio. The results are shown in Figure 7. The natural gas scheduling and utilization patterns are very similar between the solar-dominated portfolio reported in the manuscript and the wind-dominated portfolio shown here. The most prominent difference between the two scenarios arises in the diurnal cycle of the natural gas utilization. Both portfolios tend to require more natural gas reserves at night, when solar power is

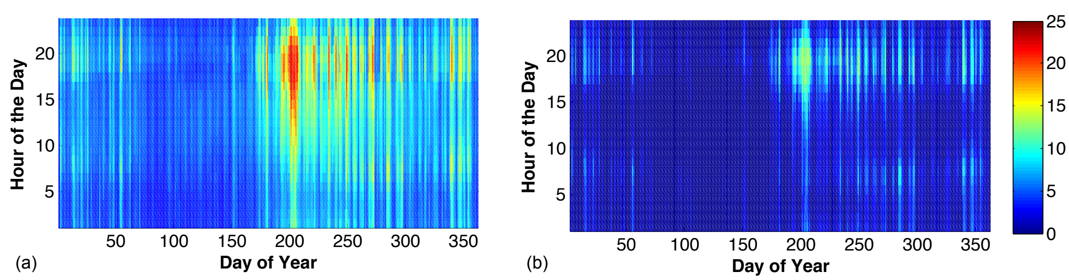

Figure 7 The average (a) available, and (b) utilized natural gas generating capacity in each hour of the year for a simulation of the California ISO over 2005-2006 with a renewable portfolio consisting of 70GW wind, 30GW solar, and 9GW geothermal power.

Electronic Supplementary Material (ESI) for Energy & Environmental Science
This journal is © The Royal Society of Chemistry 2012

unavailable, however this trend is more prominent in the solar-dominated portfolio because the daytime natural gas utilization is reduced due to an excess of day-time solar power.

References

[Hart and Jacobson(2011)] Hart EK, Jacobson MZ. A Monte Carlo approach to generator portfolio planning and carbon emissions assessments of systems with large penetrations of variable renewables. Renewable Energy 2011;36(8):2278 – 2286.

[3TIER(2010)] 3TIER . Wind integration datasets. `www.nrel.gov/wind/integrationdatasets`; 2010.

[Wilcox and Marion(2007)] Wilcox S, Marion W. National solar radiation database, 1999 - 2005: User's manual. Technical Report TP-581-41364; National Renewable Energy Laboratory; 2007. URL `http://www.nrel.gov/docs/fy07osti/41364.pdf`.

[Clean Power Research, LLC(2010)] Clean Power Research, LLC . SolarAnywhere. `www.solaranywhere.com`; 2010.

[Mancini(2011)] Mancini T. Operation of parabolic trough solar power plants. 2011. Personal Communication.